A Quantitative Analysis of the Enhanced-V Feature in Relation to Severe Weather

JASON C. BRUNNER, STEVEN A. ACKERMAN, AND A. SCOTT BACHMEIER

Cooperative Institute for Meteorological Satellite Studies, University of Wisconsin—Madison, Madison, Wisconsin

ROBERT M. RABIN

National Oceanic and Atmospheric Administration/National Severe Storms Laboratory, Norman, Oklahoma

(Manuscript received 1 December 2005, in final form 17 November 2006)

ABSTRACT

Early enhanced-V studies used 8-km ground-sampled distance and 30-min temporal-sampling Geostationary Operational Environmental Satellite (GOES) infrared (IR) imagery. In contrast, the ground-sampled distance of current satellite imagery is 1 km for low earth orbit (LEO) satellite IR imagery. This improved spatial resolution is used to detect and investigate quantitative parameters of the enhanced-V feature. One of the goals of this study is to use the 1-km-resolution LEO data to help understand the impact of higher-resolution GOES data (GOES-R) when it becomes available. A second goal is to use the LEO data available now to provide better severe storm information than GOES when it is available. This study investigates the enhanced-V feature observed with 1-km-resolution satellite imagery as an aid for severe weather warning forecasters by comparing with McCann's enhanced-V study. Therefore, verification statistics such as the probability of detection, false alarm ratio, and critical success index were calculated. Additionally, the importance of upper-level winds to severe weather occurrence will be compared with that of the quantitative parameters of the enhanced-V feature. The main goal is to provide a basis for the development of an automated detection algorithm for enhanced-V features from the results in this study. Another goal is to examine daytime versus nighttime satellite overpass distributions with the enhanced-V feature.

1. Introduction and background

Many studies have observed and analyzed the enhanced-V feature (McCann 1983; Negri 1982; Heymsfield et al. 1983a,b; Heymsfield and Blackmer 1988; Adler et al. 1985). Enhanced longwave infrared (IR) satellite imagery of deep convection sometimes display this cloud-top V-shaped feature, in which an equivalent blackbody temperature (BT) region of a storm is enclosed by a V-shaped region of colder BT (see Fig. 1a; Negri 1982; McCann 1983; Heymsfield et al. 1983a,b; Fujita 1982). The enhanced-V develops when a strong updraft penetrates into the lower stratosphere and results in an overshooting thunderstorm top. This overshooting top acts to block strong upper-level winds and forces the flow to divert around it (Fujita 1978; Wang 2007). As the flow is diverted around the overshooting top, the main hypothesis is that the flow erodes the updraft summit and carries cloud debris downwind (McCann 1983). The carrying of cloud debris downwind is reflected in the colder BTs of the enhanced-V feature (McCann 1983). The coldest BT, which is near the apex of the enhanced V, is associated with adiabatic expansion due to the ascent of air parcels in the thunderstorm updraft region overshooting the tropopause (Heymsfield and Blackmer 1988; Adler and Mack 1986). Several hypotheses have been proposed to explain the warm region of BTs enclosed by the V feature. One hypothesis argues that the region is a result of subsidence of negatively buoyant overshooting cloud air downstream of an ascending cloud top (Heymsfield and Blackmer 1988; Adler and Mack 1986; Heymsfield et al. 1983a; Negri 1982; Schlesinger 1984). A second hypothesis has been proposed that explains the warm region on the basis of the radiative properties of the cloud particles. Based on radiative transfer simulations and assuming that the ice water content varied spatially across the anvil, Heymsfield et al. (1983b) found that

Corresponding author address: Jason C. Brunner, CIMSS, University of Wisconsin—Madison, Madison, WI 53706.
E-mail: jasonb@ssec.wisc.edu

DOI: 10.1175/WAF1022.1

© 2007 American Meteorological Society

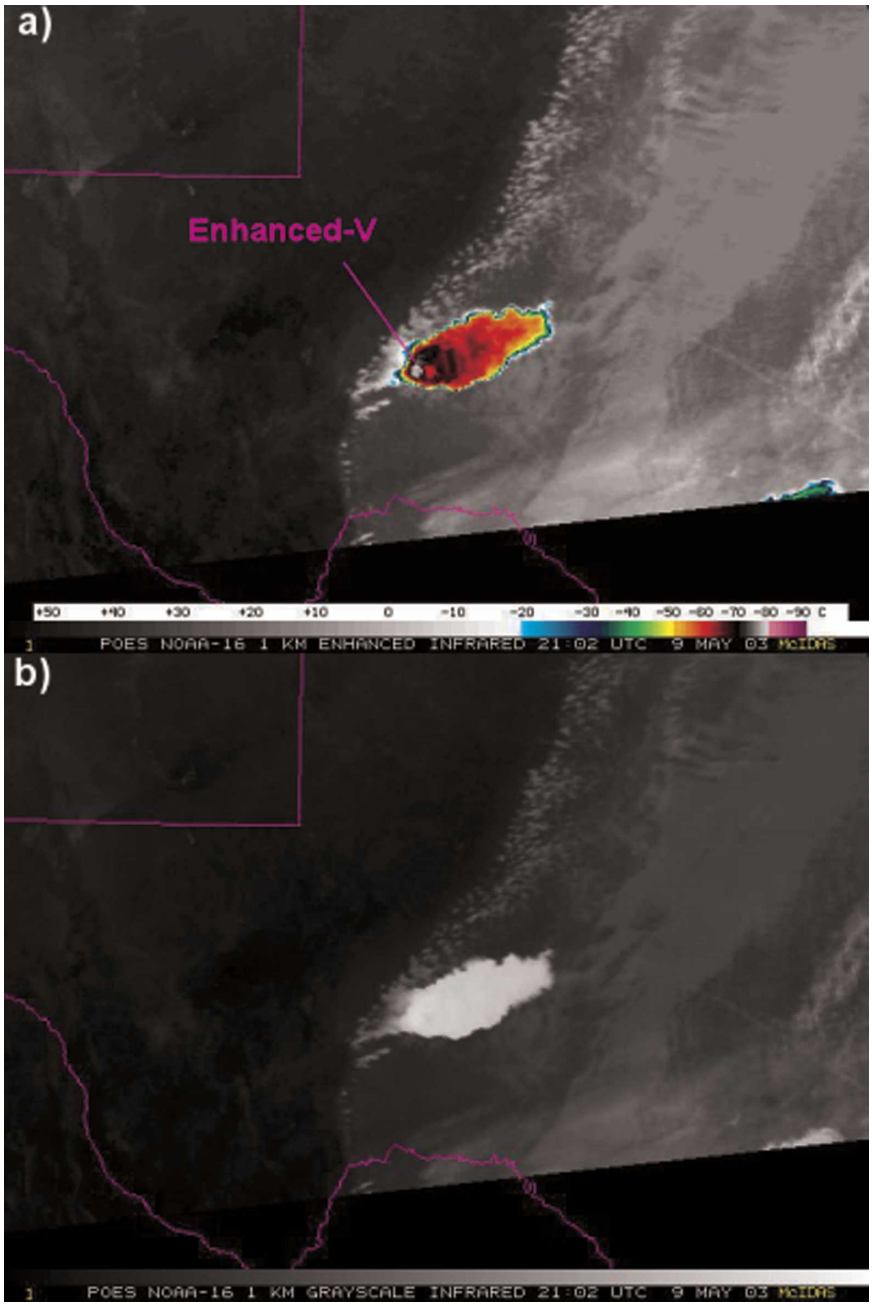

FIG. 1. A deep convective storm with an enhanced-V over southwestern TX from the LEO NOAA AVHRR 1-km spatial resolution 10.8-μm IR channel image at 2102 UTC 9 May 2003: (a) color-enhanced image and (b) black and white image.

the interior warm region had lower ice water content compared to the V's arms. This situation implies a smaller optical depth in the warm region and warmer BTs characteristic of lower altitudes. Another hypothesis argues that stratospheric cirrus (Fujita 1982) generated in the wake of overshooting tops is sinking into the anvil. Located above an anvil top and at a warmer environmental temperature, the stratospheric cirrus appears warmer in the BTs sensed by the IR satellite channel (Wang et al. 2002; Setvak et al. 2007). A fourth hypothesis describes gravity waves and lee waves produced by the storms as the cause of the warm region downwind of the coldest BT (Stobie 1975; Heymsfield et al. 1991; Wang 2007).

Two distinct types of warm regions have been identified: close-in warm areas (CWAs) and distant warm

areas (DWAs) farther downwind (Heymsfield et al. 1983a). The CWA and the coldest point of the enhanced-V form a cold-warm couplet (McCann 1983; Heymsfield et al. 1983a,b; Negri 1982; Fujita 1982). A DWA is more transient than the CWA and usually has no distinct maxima of BT (Heymsfield et al. 1983a). Five Severe Environmental Storms and Mesoscale Experiment (SESAME) cases were performed during 1979 for a Geostationary Operational Environmental Satellite (GOES) quantitative study of the enhanced V (Heymsfield and Blackmer 1988). It was found that the cold-warm couplet ranged from 7° to 17°C. The distance from the cold point to the CWA was 21–44 km and the distance from the cold point to the DWA was 40–120 km. Compared to the CWA, the DWA occurred less frequently and consisted of a larger transient area when present.

The presence of enhanced-V features signifies strong tropospheric shear and intense updrafts, both of which are also essential for severe thunderstorms (Heymsfield and Blackmer 1988). The presence of enhanced Vs is associated with severe weather (McCann 1983; Negri 1982; Heymsfield et al. 1983a,b; Adler et al. 1985; Heymsfield and Blackmer 1988). McCann (1983) explored the association of enhanced Vs to severe weather reports, suggesting a possible application for severe weather warnings. He found a 30-min median lead time from the time the enhanced V appeared in enhanced IR imagery to the time of the first report of severe weather. In addition, he found that most of the enhanced Vs studied were associated with severe weather (i.e., low false alarm ratio, FAR). However, a large number of severe storms did *not* have an enhanced V (low probability of detection, POD).

Most of these early studies of enhanced-V features and their relation to severe weather have used GOES IR imagery with 8-km ground-sampled distance and a sampling interval of 30 min. The current GOES IR imagery has a ground-sampled distance of approximately 4 km and improved temporal sampling over the continental United States region (Menzel and Purdom 1994). Low earth orbit (LEO) satellite IR imagery has a ground-sampled distance of 1 km but with limited temporal sampling. A few studies have utilized LEO satellite IR imagery to investigate enhanced-V features (Adler et al. 1983). Primarily because of the coarse resolution, GOES IR imagery overestimates the cold area BTs by about +15 K for mature thunderstorms and +30 to +40 K for small growing storms compared to LEO satellite IR imagery (Adler et al. 1983). The magnitude of the cold–warm couplet increases dramatically with LEO satellite imagery, making it easier to detect. Therefore, it is expected that the number of detectable enhanced Vs will be greater with finer-resolution imagery such as from the current LEO satellite. To date, there has not been a detailed LEO dataset of enhanced-V cases developed.

One of the goals of this study is to use the 1-km ground-sampled distance LEO data to help understand the impact of higher-resolution GOES data (GOES-R) when it becomes available. A second goal is to use the LEO data available now to provide better severe storm information than GOES when it is available. This study investigates the enhanced-V feature observed with 1-km-resolution satellite imagery as an aid for severe weather warning forecasters by comparing with McCann's enhanced-V study (McCann 1983). Therefore, verification statistics such as the POD, FAR, and critical success index (CSI) were calculated. Additionally, the importance of upper-level winds to severe weather occurrence will be compared to that of the quantitative parameters of the enhanced-V feature. The main goal is to provide a basis for the development of an automated detection algorithm for enhanced-V features from the results in this study. Another goal is to examine daytime versus nighttime satellite overpass distributions with the enhanced-V feature.

Section 2 discusses the data used in this study, while section 3 describes the enhanced-V quantitative parameters and investigates the accuracy of the parameters through an error analysis. Section 4 provides a comparison of the verification statistics with the McCann (1983) enhanced-V study. Section 5 compares the importance of upper-level winds and the quantitative parameters of the enhanced-V feature to severe weather occurrence. Also, a basis for the development of an automated detection algorithm for enhanced-V features is provided in section 5. In addition, section 5 discusses geographic and daytime versus nighttime satellite overpass distributions of enhanced-V features. Conclusions are discussed in section 6.

2. Data

Two LEO satellite datasets that included the 10.7-, 10.8-, and 11-μm IR channels were obtained over the continental United States for the enhanced-V study. These satellite datasets provide a 1-km ground-sampled distance and consisted of the following elements.

- Overpasses from the LEO National Oceanic and Atmospheric Administration (NOAA) Advanced Very High Resolution Radiometer (AVHRR) and National Aeronautics and Space Administration (NASA) Earth Observing System's (EOS) Moderate Resolution Imaging Spectroradiometer (MODIS) on

board the *Aqua* and *Terra* satellites were obtained from 4 May 2003 to 5 July 2003. There were 209 enhanced-V cases collected in the 2003 season.

- Overpasses from the LEO NOAA AVHRR and NASA EOS MODIS *Aqua* and *Terra* satellites were obtained from 1 May 2004 to 1 July 2004. There were 241 enhanced-V cases collected in the 2004 season.

The 10.8- and 11-μm IR calibration accuracy is within 1K for all AVHRR data (Gunshor et al. 2004) and within 0.3 K for MODIS (Tobin et al. 2006) satellites used in this study. The accuracy of the temperature measurements is not expected to affect significantly the evaluation of the parameters associated with enhanced-V features.

In addition, GOES water vapor–derived winds (WVDW) were used to estimate upper-tropospheric winds near 300 mb with a temporal sampling of 30 min (Rabin et al. 2004). However, use of the WVDW does not facilitate the calculation of the vertical shear. Archived rawinsonde observations (raobs) were used if the GOES WVDW data were not available at or near the time of the enhanced-V cases. Obviously, the temporal and spatial resolutions are much better with GOES WVDW than with raobs.

The Man Computer Interactive Data Access System (McIDAS) was used to display and analyze the satellite imagery (Lazzara et al. 1999).

Severe weather reports during the time periods of the enhanced-V seasons were examined. The severe reports from both seasons were obtained from the National Climatic Data Center (NCDC) publication *Storm Data* (SDP).

3. Classification of the enhanced-V in satellite observations

Enhanced-V features are associated with deep convection, which usually lasts on the order of a few hours. Therefore, since each LEO satellite has only one ascending and one descending overpass per day at any given location on Earth, the temporal nature of enhanced-V features is difficult to determine from LEO satellite imagery.

To facilitate the detection of the enhanced V (cf. Figs. 1a and 1b), the IR imagery is color enhanced based from the two-ramp dogleg scheme (historical MB enhancement curve) for converting scene temperatures into an unsigned eight-bit integer (count) in the range 0–255 (Clark 1983; Brunner 2004).

a. Enhanced-V parameters

The enhanced V can be described by the following seven parameters.

1) TMIN represents the minimum cloud-top equivalent blackbody temperature (BT) observed from the satellite. TMIN is usually near the apex of the enhanced V and is associated with adiabatic expansion owing to air parcels in the thunderstorm updraft region overshooting the tropopause (Heymsfield and Blackmer 1988; Adler and Mack 1986). The latitude and longitude of TMIN were recorded and used as the reference position of each enhanced V.
2) TMAX is the maximum cloud-top BT detected within an embedded warm area downwind of TMIN. Refer to Fig. 2a for an example of TMIN and TMAX. For this enhanced-V case, TMIN and TMAX were observed to have values of 192 K (−81°C) and 212 K (−61°C), respectively.
3) TDIFF is the difference in cloud-top BTs between TMIN and TMAX, which forms a cold–warm couplet (McCann 1983; Heymsfield et al. 1983a,b; Negri 1982; Fujita 1982).
4) DIST represents the distance between TMIN and TMAX. Refer to Fig. 2b for an example of TDIFF and DIST. For this case, TDIFF and DIST were observed to have values of 20 K and 7 km, respectively.
5) DISTARMS shows the distance of the V arms. The V arms extend outward in a V-like pattern from an apex point. Usually, the apex point is denoted as TMIN, and the farther away from the apex of the V, the warmer the cloud-top BTs. The apex of the V does not always correspond to TMIN, but is the coldest cloud-top BT along the V arms. DISTARMS was calculated for each enhanced V by averaging the two V-arm distances together. The distance of each V arm was calculated by using the McIDAS software to measure the distance between the apex point and the point on the V arm where a noticeable increase in the cloud-top BT occurred. This noticeable increase varied for each enhanced V, but was roughly a 10% change between the temperature at the apex point and the temperature at the end of the V arm.
6) ANGLEARMS shows the angle between the two V arms. Refer to Fig. 2c for an example of DISTARMS and ANGLEARMS. DISTARMS and ANGLEARMS were observed to have values of 22.5 km and 72°, respectively.
7) ORIENTATION is the orientation of the enhanced V. For simplicity, the ORIENTATION parameter is categorized by four 90° quadrants—southwest, northwest, northeast, and southeast. The quadrant(s) that each enhanced V was assigned to is determined by two criteria. First, the quadrant that contains the highest number of degrees of the en-

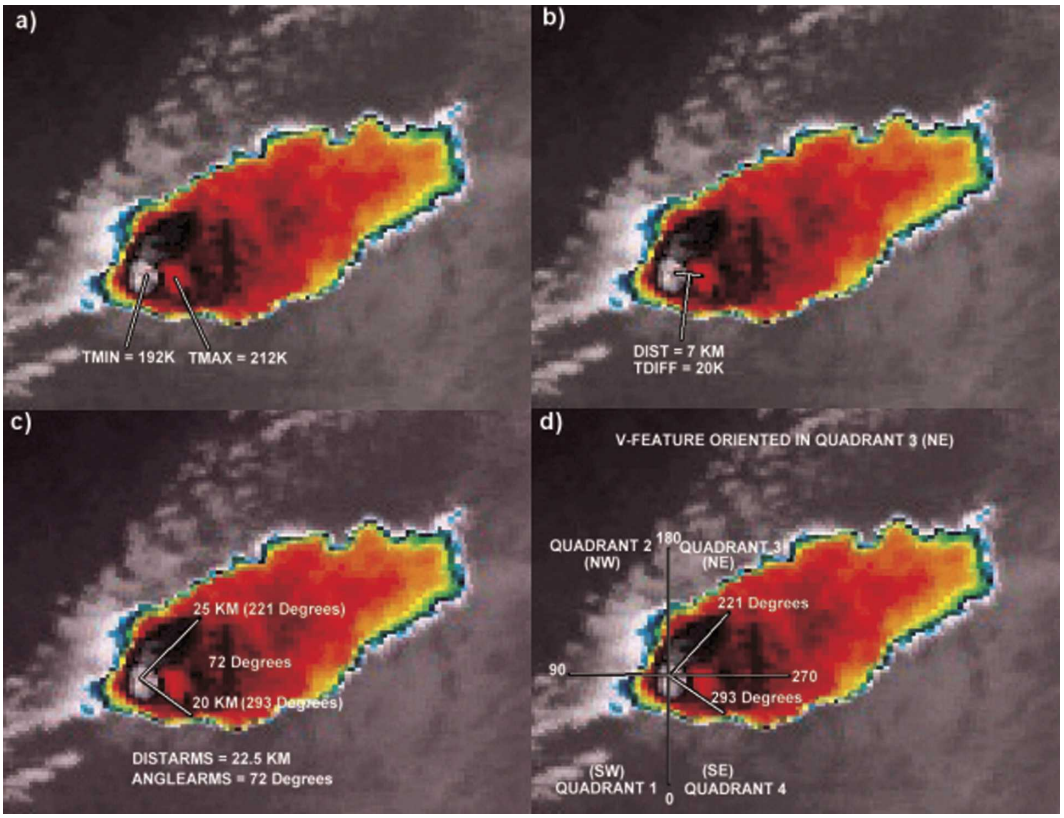

FIG. 2. A zoomed-in LEO NOAA AVHRR 1-km spatial resolution enhanced 10.8-μm IR channel image over southwestern TX at 2102 UTC 9 May 2003. The enhanced-V quantitative parameters are labeled as (a) TMIN (K) and TMAX (K), (b) TDIFF (K) and DIST (km), (c) DISTARMS (km) and ANGLEARMS (°), and (d) ORIENTATION.

hanced V is counted. Second, each quadrant that contains 45° or more is counted. However, a quadrant was not counted more than once for each enhanced V. Refer to Fig. 2d for an example of the quantitative parameter ORIENTATION. For this enhanced-V case, the enhanced-V orientation was determined to be the northeast quadrant because there were 49° of angle present in the northeast quadrant, while only 23° of angle were present in the southeast quadrant.

For the southwestern Texas enhanced-V case discussed earlier, the upper-level wind speed was estimated at 65 kt (33 m s^{-1}) and the upper-level wind direction was toward the northeast.

The enhanced-V parameters TMIN, TMAX, and TDIFF were compared at different ground-sampled distances from LEO satellite imagery for an enhanced-V case to see if varying the ground-sampled distance has an effect on these parameters. The enhanced-V feature was observed at 1-, 2-, 4-, and 8-km ground-sampled distances from LEO satellite imagery and is shown in Fig. 3. The TMIN enhanced-V parameter got warmer as the ground-sampled distance got coarser (i.e., 4 and 8 km; Table 1). In fact, TMIN was observed to be 11 K warmer for the LEO 8-km ground-

TABLE 1. The BT values for the enhanced-V parameters TMIN, TMAX, and TDIFF for an enhanced-V feature observed from LEO satellite imagery at 1-, 2-, 4-, and 8-km ground-sampled distances over northeast OK at 2218 UTC 6 May 2003.

Enhanced-V parameter	1-km ground-sampled distance	2-km ground-sampled distance	4-km ground-sampled distance	8-km ground-sampled distance
TMIN	186 K (−87°C)	188 K (−85°C)	193 K (−80°C)	197 K (−76°C)
TMAX	219 K (−54°C)	218 K (−55°C)	216 K (−57°C)	215 K (−58°C)
TDIFF	33 K	30 K	23 K	18 K

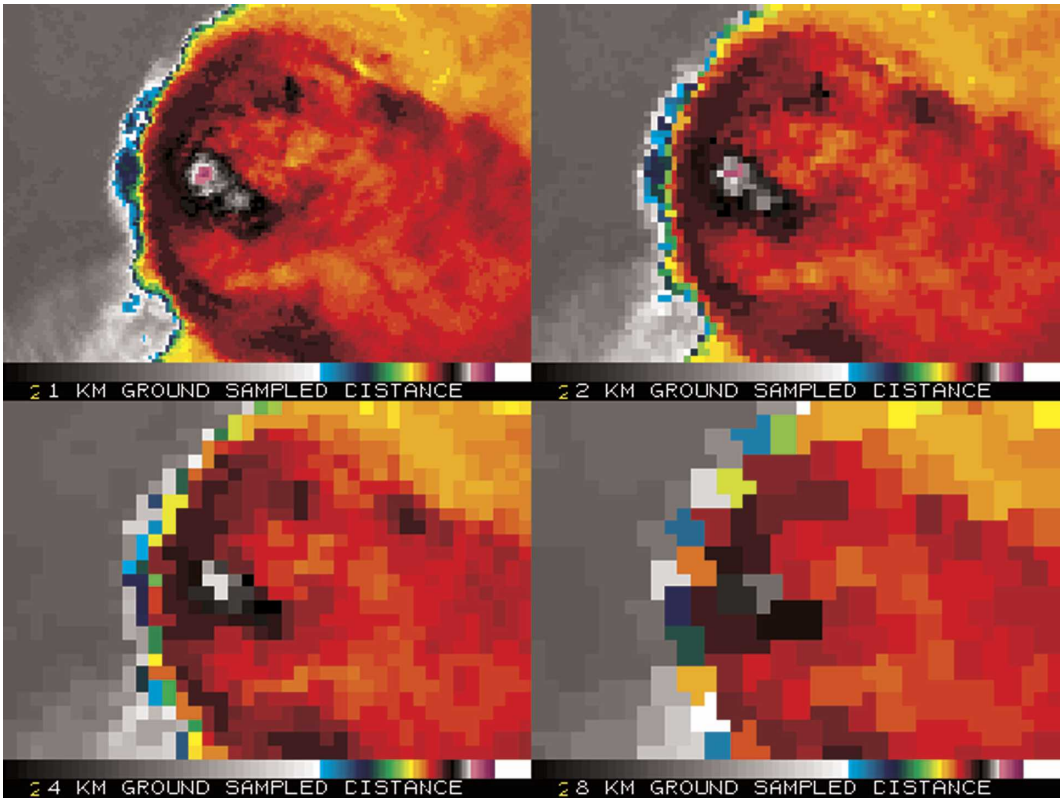

FIG. 3. Zoomed-in image of an enhanced-V feature located over northeast OK observed from enhanced LEO satellite imagery at 2218 UTC 6 May 2003 for 1-, 2-, 4-, and 8-km ground-sampled distances. The purple and white colors in the location of the updraft and overshooting top represent colder BTs, while the surrounding black and red colors represent warmer BTs.

sampled distance compared to the LEO 1-km ground-sampled distance. The warmer TMIN values were observed for the 4- and 8-km ground-sampled distances because at these ground-sampled distances, the satellite imagery could not resolve the overshooting top regions adequately. However, since the average diameter of an overshooting top is between 1 and 2 km, satellite imagery observed at 1- and 2-km ground-sampled distances could resolve the overshooting top regions adequately and hence observed colder TMIN values at these finer ground-sampled distances. The TMAX parameter values got slightly colder for coarser LEO ground-sampled distances, but only changed by 4 K from 1- to 8-km ground-sampled distances (Table 1). This seems to be because the temperature region associated with TMAX occurs over a relatively large area (compared to TMIN) and can be resolved fairly well for both finer (1 km) and coarser (8 km) ground-sampled distances. The TDIFF parameter values decreased significantly (15 K) from finer (1 km) to coarser (8 km) LEO ground-sampled distance (Table 1). These temperature couplet value changes were affected mainly by TMIN since the value of TMAX did not change much from LEO at 8- to 1-km ground-sampled distances.

b. *Error analysis of enhanced-V parameters*

Since the technique that identifies and analyzes the enhanced-V quantitative parameters is somewhat subjective, the uncertainty of the parameters was tested. A subsample consisting of approximately 10% of the enhanced-V cases from the 2003 season was randomly selected by a second analyst. For each enhanced-V case that was selected for the reanalysis, the seven quantitative parameters were determined and compared to the results from the original analysis of the parameters determined from the first analyst.

For each enhanced-V parameter (excluding the ORIENTATION parameter), the mean of the first analysis and the reanalysis were calculated (Table 2). In addition, the percent difference between analysts was calculated for the mean for each parameter. These percent differences show that measuring equivalent blackbody temperatures was more accurate than measuring distances and angles of the enhanced-V param-

TABLE 2. The mean values of the first analysis and the reanalysis for the enhanced-V parameters TMIN, TMAX, TDIFF, DIST, DISTARMS, and ANGLEARMS. Also shown is the percent difference for the mean value between the first analysis and the reanalysis for each enhanced-V parameter.

Enhanced-V parameter	First analysis	Reanalysis	Percent difference
TMIN (K)	199.6	199.8	0.1
TMAX (K)	215.8	216.9	0.5
TDIFF (K)	16.2	17.2	6.3
DIST (km)	10.3	19.0	87.0
DISTARMS (km)	32.9	41.1	24.8
ANGLEARMS (°)	79.6	70.9	10.9

eters. The measurements of DIST, DISTARMS, and ANGLEARMS are more subjective than the measurements of TMIN, TMAX, and TDIFF.

The ORIENTATION parameter was also analyzed. The southwest and northwest quadrant percentages did not change. However, the northeast quadrant percentages were overestimated by 12%, while the southeast quadrant percentages were underestimated by 6% for the reanalysis. These differences are dictated by the ANGLEARMS parameter and lead to differences in the ORIENTATION parameter by shifting the direction toward that in which the enhanced V is oriented. Overall, since the percent differences for the mean for ANGLEARMS was relatively small (i.e., 10.9%), the percent differences for ORIENTATION were also relatively small (largest difference was 12%).

The number of enhanced-V cases identified by each analyst was also compared. The person who did the reanalysis determined that 3 of the 20 cases in this error analysis were not considered enhanced-V features in their judgment, while the same three cases were considered enhanced-V features by the person who did the original analysis. Therefore, determining if an area of deep convection has an enhanced-V feature associated with it can be problematic and quite subjective at times, especially in marginally enhanced-V case scenarios where the enhanced-V feature is quite subtle in the imagery. In addition, using LEO satellite imagery to determine if a feature is actually an enhanced V can be difficult in the marginally enhanced-V cases because of the coarse temporal sampling of the LEO satellite imagery. For the three questionable enhanced-V cases discussed above, the person who did the reanalysis determined that two of the cases had "warm trenches" observable from the LEO imagery. Warm trench features consist of a colder temperature region, such as TMIN, surrounded entirely by warmer BTs. It is hypothesized that the warm trench (cloud trench) occurs near the storm summit as observed in Fujita (1974), which supports a subsiding flow pattern downwind of the storm summit due to adiabatic compression. The warm trench cases in general may be associated with severe weather, although no detailed studies have investigated the warm trench in relation to severe weather. Future studies should investigate the warm trench to see if there are any relationships to severe weather.

4. Enhanced-V comparison with the McCann (1983) study

One of the goals of this study is to investigate the enhanced-V feature observed with finer ground-sampled distance (i.e., 1 km) satellite imagery as an aid for severe weather warning forecasters and to compare with McCann's (1983) enhanced-V study. Therefore, verification statistics such as the probability of detection (POD), false alarm ratio (FAR), and critical success index (CSI) were calculated. The POD is defined as the ratio of the number of events N that are correctly forecasted to occur to the total number of events T (Schaefer 1990):

$$\mathrm{POD} = N/T.$$

The FAR is defined as the ratio of the number of false alarms F to the total number of predicted events P (Schaefer 1990):

$$\mathrm{FAR} = F/P.$$

Finally, the CSI is defined in terms of the FAR and POD (Schaefer 1990):

$$\mathrm{CSI} = [(\mathrm{POD})^{-1} + (1 - \mathrm{FAR})^{-1} - 1]^{-1}.$$

In this study, the presence of an enhanced-V feature during the LEO overpass indicates a severe storm warning. The POD is defined then as the ratio of the number of enhanced-V features that were actually associated with severe weather to the total number of severe storms. The FAR is defined then as the ratio of the number of enhanced-V features that did not have severe weather associated with them to the total number of enhanced-V features. Since this study deals with LEO satellite imagery, severe storms and enhanced-V features that were not present in the LEO satellite imagery, but that may have occurred at other times or in different regions other than the overpass swath/time, were not included in this study. LEO overpasses from 4 May to 5 July 2003 and 1 May to 1 July 2004 were analyzed for enhanced-V features.

Each enhanced-V feature minimum equivalent blackbody temperature (TMIN) location was plotted in the satellite image with a 60-km circular radius outlined

around it. As discussed later, this circular outline denotes the distance threshold chosen to determine if a severe report is associated with an enhanced-V feature. If a severe report is located within the circular radius of the enhanced-V feature, then it is assumed to be associated with the enhanced V. However, if the severe report is located outside of the circular radius, then it is assumed to be associated with a different storm. For events in both years, these severe reports included hail greater than or equal to 0.75-in. diameter, winds greater than or equal to 58 mi h^{-1} (50 kt), and tornadoes. In addition, significant severe reports were plotted, which consisted of hail reports greater than or equal to 2.00-in. diameter, winds greater than or equal to 80 mi h^{-1} (70 kt), and F2–F5 tornadoes. Severe reports from 30 min before the overpass time to 30 min after the overpass time were plotted in the same satellite image. McCann used GOES imagery over the entire United States from April to July in his study and included severe reports within 60 min after an enhanced V. In this study, a 60-min time range was used for severe reports to be consistent with the results of McCann. However, the endpoints of the range were chosen to be 30 min before to 30 min after the overpass time because it was felt that a time within 30 min of the overpass would represent the severe reports adequately in relation to the LEO overpass image owing to time evolution of storms. In addition, the time range must be large enough to account for errors in reporting times of severe weather.

The distance of 60 km was chosen as the threshold for the following reasons. First, since there is a 1-h time range in this study for the severe reports, time evolution of a storm must be taken into consideration. Even for extreme cases when a storm is moving faster than 100 km h^{-1}, the 60-km radius would capture the storm. Second, the coldest point of a thunderstorm as observed from satellite can be offset upwind from the highest point of a thunderstorm. This offset can be 10 km or more in some cases (Adler and Mack 1986). Third, the updraft may slope vertically. For example, the displacement distance between the top and base of a thunderstorm updraft was found to be between 15 and 20 km (Heymsfield et al. 1983a). Therefore, even though the satellite is observing TMIN at a certain location, the base of a thunderstorm updraft and the severe reports can be displaced a substantial distance from TMIN. Also, parallax can affect the projected ground location of the severe reports. The size of the parallax error depends on the height and location of the cloud relative to the satellite. Finally, severe hail and winds can be displaced a large distance from the main updraft–downdraft location of a storm. For example, Miller et al. (1990) showed hail-producing regions extending 10–15 km to the east-southeast of the updraft locations. There also seemed to be multiple hail-producing regions in/around the updraft location. Also, severe winds that are produced along gust fronts can propagate very long distances from a parent thunderstorm. It is expected that the 60-km circular radius is large enough to capture the displacements of most severe reports due to storm motion and structure; however, severe reports may be misrepresented as being associated with an enhanced-V feature in the case of closely spaced or multicellular storms where updrafts are less than 120 km apart. McCann (1983) did not specify a distance threshold around an enhanced-V feature for inclusion of severe reports in his study.

Two techniques were used to calculate the POD for each season with respect to this enhanced-V polar orbiting overpass study. The first technique is the "no storm definition" POD, where all severe reports were included in the POD without regard to the presence of a storm in the satellite imagery at the time of the LEO overpass. Severe reports of the same type (e.g., hail, wind, or tornado) within 60 km of each other outside of the enhanced-V circular radius outlines were grouped together and counted only once in the POD calculation, just as each enhanced-V feature with multiple severe reports of the same type was counted only once. The second technique is the "storm definition" POD, where only severe reports were included in the POD if the severe report was within 60 km of a satellite pixel with a BT of −47°C (226 K) or colder. It was performed to exclude possible situations of rapid storm growth when full storm development may have occurred just after the satellite overpass time with severe weather occurring within 30 min. A BT threshold of −47°C was chosen because Adler et al. (1985) used this value as a determining factor for a definition of a thunderstorm. Also, homogeneous nucleation occurs around −40°C, which is a good indication of higher-level/more pronounced vertical cloud development compared to lower- to middle-level cloud development.

The 2003 POD values (Table 3) for the storm definition technique are within 1% of those from the no storm definition technique for both tornado and wind severe types. However, for hail, the storm definition POD is 3% higher for severe hail and 8% higher for significant severe hail. The 2004 season POD values for the storm definition technique are 1% higher for the severe types of hail and tornado compared to the no storm definition technique, while the severe type of wind is 3% higher. All significant severe types for the 2004 season POD values were within 3%. The 2004 season POD values showed that the storm definition

TABLE 3. The POD values (N/T) for the 2003 and 2004 seasons for severe (SVR) wind, SVR hail, tornado, averaged for all SVR types (total), significant (SIG) SVR wind, SIG SVR hail, SIG tornado, and averaged for all SIG SVR types (total). The two POD techniques are "no storm definition" and "storm definition." Here, storm definition corresponds to severe reports within 60 km of −47°C equivalent blackbody temperature pixel values. Numbers in parentheses represent N divided by T.

	SVR wind	SVR hail	Tornado	Avg (total) for SVR types	SIG SVR wind	SIG SVR hail	SIG tornado	Avg (total) for SIG SVR types
No storm definition POD, 2003 season	57/257 (0.22)	124/445 (0.28)	64/136 (0.47)	245/838 (0.29)	4/22 (0.18)	23/49 (0.47)	15/30 (0.5)	42/101 (0.42)
Storm definition POD, 2003 season	57/244 (0.23)	124/396 (0.31)	64/133 (0.48)	245/773 (0.32)	4/21 (0.19)	23/42 (0.55)	15/30 (0.5)	42/93 (0.45)
No storm definition POD, 2004 season	49/256 (0.19)	156/447 (0.35)	33/85 (0.39)	238/788 (0.30)	5/21 (0.24)	22/38 (0.58)	3/10 (0.30)	30/69 (0.43)
Storm definition POD, 2004 season	49/227 (0.22)	156/429 (0.36)	33/82 (0.40)	238/738 (0.32)	5/19 (0.26)	22/38 (0.58)	3/9 (0.33)	30/66 (0.45)

TABLE 4. The POD values (N/T) from McCann's (1983) enhanced-V study, which includes the ratio of severe reports within 60 min after an enhanced V to all severe reports, ratio of tornadoes verified, and ratio of F2–F5 tornadoes verified for April, May, June, July, and the total. Numbers in parentheses represent N divided by T.

	Apr	May	Jun	Jul	Tot
Ratio of severe reports within 60 min after an enhanced V to all severe reports	140/504 (0.28)	173/565 (0.31)	189/925 (0.20)	143/725 (0.20)	645/2719 (0.24)
Ratio of tornadoes verified	31/119 (0.26)	38/111 (0.34)	19/149 (0.13)	13/132 (0.10)	101/511 (0.20)
Ratio of F2–F5 tornadoes verified	22/40 (0.55)	10/15 (0.67)	6/14 (0.43)	0/7 (0.00)	38/76 (0.50)

TABLE 5. The FAR values (F/P) for the 2003 and 2004 seasons for SVR wind, SVR hail, tornado, any SVR type, SIG SVR wind, SIG SVR hail, SIG tornado, and any SIG SVR type. Numbers in parentheses represent F divided by P.

	SVR wind	SVR hail	Tornado	Any SVR type	SIG SVR wind	SIG SVR hail	SIG tornado	Any SIG SVR type
FAR, 2003 season	152/209 (0.73)	85/209 (0.41)	145/209 (0.69)	77/209 (0.37)	205/209 (0.98)	194/209 (0.93)	194/209 (0.93)	180/209 (0.86)
FAR, 2004 season	196/241 (0.81)	107/241 (0.44)	211/241 (0.88)	88/241 (0.37)	234/241 (0.97)	219/241 (0.91)	238/241 (0.99)	213/241 (0.88)

TABLE 6. FAR-related values from McCann's (1983) enhanced-V study: the ratio of enhanced Vs associated with severe weather within 60 min to all enhanced Vs (= 1 − FAR) and the FAR for April, May, June, July, and the total.

	Apr	May	Jun	Jul	Tot
Ratio and 1 − FAR (in parentheses)	110/150 (0.73)	180/241 (0.75)	185/277 (0.67)	133/216 (0.61)	608/884 (0.69)
FAR	0.27	0.25	0.33	0.39	0.31

did not impact the POD results in this study significantly. Another interesting finding was that tornadoes had higher POD values compared to hail and winds except for significant hail. In addition, significant severe types had higher POD values compared to the marginal severe types except for winds in the 2003 season and tornadoes in the 2004 season. McCann found a POD of 0.24 for severe weather in general (Table 4) and he found a POD of 0.20 for tornadoes. Comparatively, in this study PODs of 0.29 and 0.30 were found for severe weather in general for the 2003 and 2004 seasons, respectively. PODs of 0.47 and 0.39 were found for tornadoes for the 2003 and 2004 seasons, respectively. An increase to finer ground-sampled distance satellite imagery (from McCann's 8-km GOES imagery to this study's 1-km LEO imagery) may have been the cause of the improvement in the enhanced-V POD for severe weather and especially for tornadoes. McCann also looked at significant (F2–F5) tornadoes and found an increase of the POD to 50% (Table 4), which was also found in the 2003 season of this study (Table 3). However, the POD values for severe weather are still relatively low for forecasting severe weather because 50% of the time there is severe weather observed without an enhanced-V feature.

The FAR values for both the 2003 and 2004 seasons (Table 5) are smallest for severe hail, while the FAR values are largest for severe wind in the 2003 season and tornadoes in the 2004 season. Also, the FAR values are larger for significant severe types compared to marginal severe types. This is because the significant severe types do not occur as often as the marginal severe types. McCann (Table 6) found an FAR of 0.31 for severe weather in general, while the FAR in this study for severe weather in general was 0.37 for both seasons. The FAR values for severe weather prediction increased slightly, while the CSI values were slightly improved compared to McCann's study (Tables 7 and 8). If the constraint on the time of the severe reports with respect to the observation of the enhanced-V feature is loosened to be within 3 h before or after the enhanced-V image time, then the FAR values for severe weather in general decreased to values slightly better than McCann's at 0.18 and 0.22 for the 2003 and 2004 seasons, respectively. GOES data were used to observe the temporal evolution of the enhanced-V features and its associated severe weather for the FAR analysis in the loosened time constraint case because in some cases severe weather was associated with an enhanced-V feature 1–2 h before or after the image time of the LEO overpass and it was not certain if a severe report was associated with a certain enhanced-V feature observed in the LEO image alone. Therefore, GOES data were used to show the time series of the enhanced-V features for cases when severe weather occurred more than 30 min before or after the observation of the enhanced-V feature during the overpass.

The subjective uncertainty of determining if an enhanced-V feature is present in an image may play a small role in modifying the POD and FAR values found in this study. If some of the "marginally" enhanced-V cases determined by the first analyst were not considered enhanced-V cases according to the second analyst, the FAR value may slightly decrease. The slight decrease in the FAR may be explained by eliminating some of the marginally enhanced-V cases that did not have severe weather associated with them. In addition, the POD may slightly decrease by eliminating the mar-

TABLE 7. The CSI values for the 2003 and 2004 seasons for SVR wind, SVR hail, tornado, any SVR type, SIG SVR wind, SIG SVR hail, SIG tornado, and any SIG SVR type. CSI values are calculated with both POD techniques for each season.

	SVR wind	SVR hail	Tornado	Any SVR type	SIG SVR wind	SIG SVR hail	SIG tornado	Any SIG SVR type
CSI with no storm definition POD, 2003 season	0.14	0.23	0.23	0.25	0.02	0.10	0.07	0.12
CSI with storm definition POD, 2003 season	0.14	0.26	0.23	0.27	0.02	0.10	0.07	0.12
CSI with no storm definition POD, 2004 season	0.11	0.27	0.10	0.26	0.03	0.08	0.01	0.10
CSI with storm definition POD, 2004 season	0.11	0.28	0.10	0.27	0.03	0.08	0.01	0.10

TABLE 8. The CSI values from McCann's (1983) enhanced-V study, for April–July and the total.

	Apr	May	Jun	Jul	Tot
CSI	0.25	0.28	0.19	0.17	0.21

ginally enhanced-V cases that were associated with severe weather.

5. Relation of enhanced-V parameters to severe weather

a. *Comparison of parameters between seasons*

Refer to Table 9 for results of the quantitative parameters of the enhanced-V feature for both seasons. The mean and median values of the enhanced-V parameters represent what the "average" enhanced V looks like in the enhanced-V seasons observed with LEO IR imagery. Also, the minimum and maximum values show what the extremes of the enhanced-V parameters look like in the enhanced-V seasons observed with LEO IR imagery. The percent differences between the two seasons for the mean and median values are largest for DIST (9% and 10%, respectively) and DISTARMS (5% and 11%, respectively), while they are smallest for TMIN (0% and 1%, respectively), TMAX (0% for both mean and median), TDIFF (0% and 6%, respectively), and ANGLEARMS (4% and 1%, respectively). These percent differences for the mean and median values of the parameters between the two seasons are fairly small, which confirms that interannual variability of the enhanced-V parameters is not that important.

TABLE 9. The mean, median, max, and min values for TMIN, TMAX, TDIFF, DIST, DISTARMS, and ANGLEARMS for the 2003 and 2004 enhanced-V seasons.

2003 season				
Parameter	Mean	Median	Max	Min
TMIN (K)	201	200	222	184
TMAX (K)	217	217	246	205
TDIFF (K)	16	16	35	5
DIST (km)	11	10	43	3
DISTARMS (km)	39	31	177	9
ANGLEARMS (°)	78	75	130	25
2004 season				
Parameter	Mean	Median	Max	Min
TMIN (K)	201	201	220	181
TMAX (K)	217	217	232	206
TDIFF (K)	16	15	41	5
DIST (km)	10	9	41	3
DISTARMS (km)	41	34.5	146.5	10
ANGLEARMS (°)	75	74	117	38

TABLE 10. Results from the ORIENTATION parameter showing the percentage of enhanced-V cases from the 2003 and 2004 seasons that were assigned to the southwest, northwest, northeast, and southeast quadrants.

Quadrant	2003 season	2004 season
Southwest	5%	1%
Northwest	10%	3%
Northeast	60%	73%
Southeast	38%	28%

The results for the ORIENTATION parameter are shown in Table 10. The northeast and southeast quadrants contained by far the highest percentages of enhanced Vs, while the southwest and northwest quadrants had much smaller percentages of enhanced Vs. This is mainly because the upper-level wind direction associated with most of the enhanced-V cases was from the southwest or northwest. In fact, 83% and 90% of the enhanced-V cases from the 2003 and 2004 seasons, respectively, had both their ORIENTATION and upper-level wind direction aligned in the same direction. However, there were several cases where the ORIENTATION and upper-level wind direction associated with the enhanced V were not aligned in the same direction. This may be explained by storm-relative winds having an impact on the direction that the enhanced V is oriented toward rather than just the upper-level wind direction at the near-tropopause level.

b. *Association of individual parameters with severe weather*

Severe weather reports were analyzed for the two enhanced-V seasons. Severe reports from 3 h before the enhanced-V image time to 3 h after the image time were included in the analysis. These severe reports included hail greater than or equal to 0.75-in. diameter, winds greater than or equal to 58 mi h^{-1} (50 kt), and tornadoes. The 2003 season is the dependent dataset, while the 2004 season is the independent dataset. Eight severe weather categories were plotted in the severe weather and enhanced-V parameter analysis:

- tornado, hail, and wind reports;
- tornado and hail reports only;
- tornado and wind reports only;
- hail and wind reports only;
- tornado report only;
- hail report only;
- wind report only; and
- no tornado, hail, or wind report.

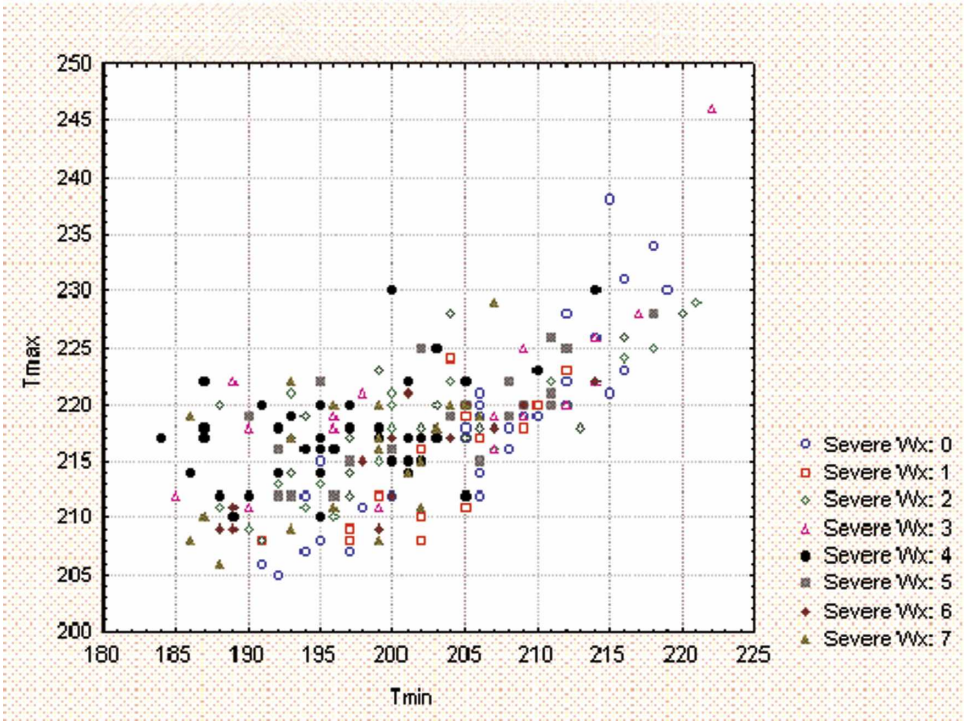

FIG. 4. A 2D scatterplot of TMIN (K) vs TMAX (K) for all enhanced-V cases in the 2003 season. Each enhanced-V case was assigned to one of eight severe weather categories: 0, no tornado, hail, or wind; 1, wind only; 2, hail only; 3, tornado only; 4, tornado, hail, and wind; 5, tornado and hail only; 6, tornado and wind only; and 7, hail and wind only.

Two-dimensional scatterplots of the severe reports associated with the enhanced-V cases were examined. The 2D scatterplots consisted of comparing two enhanced-V parameters at a time. All enhanced-V parameters were compared to each other in the scatterplots. Thresholds of the enhanced-V parameters were chosen to determine the percentage of enhanced-V cases from the 2003 season (dependent dataset) that had severe weather associated with them. Then, the same thresholds of the enhanced-V parameters were applied to the 2004 season (independent dataset) to determine and compare the percentage of enhanced-V cases that had severe weather associated with them to the 2003 season. The severe weather categories that are listed above were grouped into four simplified categories; tornado, severe hail, severe wind, and any of three severe types. The percentages of enhanced-V cases that met the thresholds for the enhanced-V parameters being compared in the 2D scatterplots and that were associated with each severe weather category were calculated.

The only 2D scatterplot that was found to have significant potential in severe weather warning decision making was TMIN versus TMAX (Figs. 4 and 5). Enhanced-V cases that had a TMIN of less than 205 K (−68°C) and a TMAX greater than or equal to 212 K (−61°C) were determined as the thresholds for the TMIN versus TMAX scatterplot. For the 2003 and 2004 seasons, 96% and 88%, respectively, of the enhanced-V cases that met the TMIN and TMAX thresholds had any of three severe types category associated with them (Table 11). Enhanced-V cases that met the TMIN and TMAX thresholds had the largest association to severe hail for both seasons, while the lowest association to severe wind and tornadoes in the 2003 season and tornadoes in the 2004 season. The percent errors between the 2003 and 2004 seasons for the TMIN versus TMAX scatterplot were largest for tornadoes and smallest for severe hail and severe wind (Table 11). Overall, the percent error between the two seasons for the TMIN versus TMAX scatterplot for any of three severe types category was 8%.

The enhanced-V parameter TMIN is associated with the updraft location of deep convection and signifies the strength of the updraft (Heymsfield and Blackmer 1988; Adler and Mack 1986). Therefore, the TMIN threshold was used to distinguish between updraft strengths; if a TMIN associated with an enhanced-V case was colder than 205 K (−68°C), it was considered a stronger updraft compared to TMIN values warmer than the 205-K (−68°C) threshold. In addition, the en-

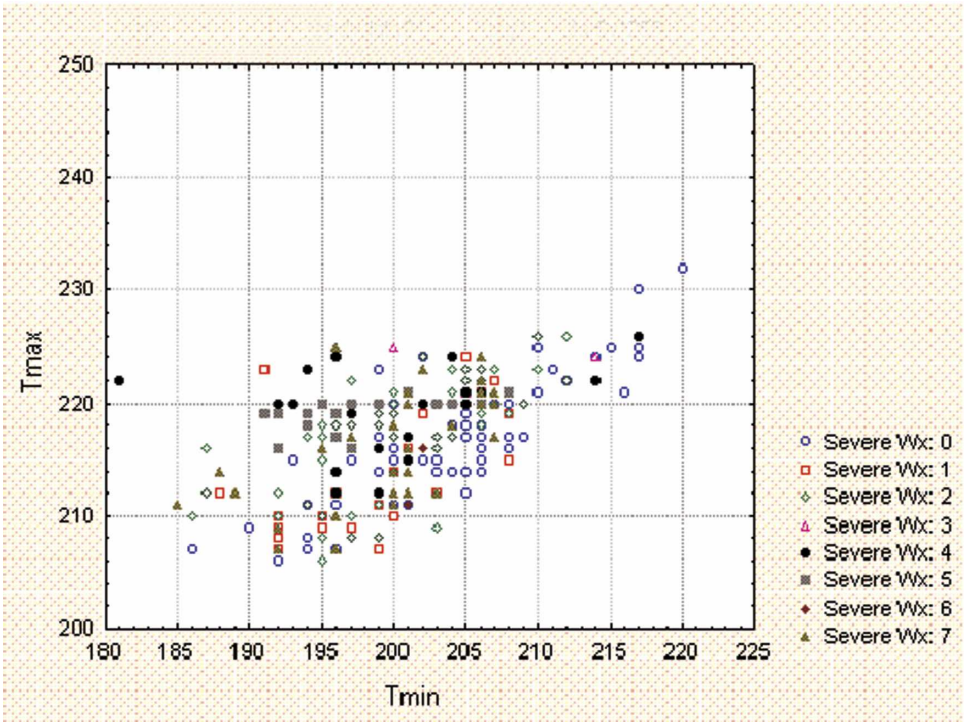

FIG. 5. Same as in Fig. 4 but for the 2004 season.

hanced-V parameter TMAX is hypothesized to be the result of various mechanisms that were discussed in the background section of this paper. One of the mechanisms proposed was TMAX resulting from adiabatic descent (subsidence) downwind of the updraft location (Heymsfield and Blackmer 1988; Adler and Mack 1986; Heymsfield et al. 1983a; Negri 1982; Schlesinger 1984). The thresholds of TMIN and TMAX combined in the scatterplot represent TDIFF because as TMIN gets colder and TMAX gets warmer, TDIFF gets larger. The larger TDIFF values represent stronger updrafts in conjunction with a warm region. The enhanced-V cases that met the TMIN and TMAX thresholds had high percentages (96% for the 2003 season and 88% for the 2004 season) of being associated with severe weather as indicated above. Therefore, a forecaster could use TMIN and TMAX in a quantitative sense to distinguish the strength of a storm and in severe weather warning decision making since these parameters are linked to the strength of physical processes in deep convection. In addition, an enhanced-V automated detection algorithm could be developed to focus on the TMIN, TMAX, and TDIFF values and provide warnings to a storm if these values exceeded thresholds of 205 K (−68°C) for TMIN and 212 K (−61°C) for TMAX (implying larger TDIFF values). Another important point is that DIST, DISTARMS, and ANGLEARMS do not seem to be important for severe weather warning decision making since there were no associations between the enhanced-V cases and severe weather found in this study for these parameters. Hence, an enhanced-V automated detection algorithm should focus mainly on the temperature parameters of the enhanced V rather than the distance of the V arms and angle separation between the V arms.

TABLE 11. Results from a 2D scatterplot of TMIN vs TMAX for enhanced-V cases that met the TMIN and TMAX thresholds and that were associated with severe weather to the total number of enhanced-V cases that met the TMIN and TMAX thresholds. The severe weather categories included tornado, hail, wind, and any of three severe types for the 2003 and 2004 seasons. Also, the percent error between the 2003 and 2004 seasons is given for each severe weather category.

Severe weather category	2003 season	2004 season	Error (%)
Tornado	54/103 (52%)	33/113 (29%)	23
Hail	82/103 (80%)	95/113 (84%)	4
Wind	54/103 (52%)	54/113 (48%)	4
Any of three severe types	99/103 (96%)	99/113 (88%)	8

A box plot of TMIN values associated with enhanced-V cases from the 2003 season for the eight severe weather categories discussed at the beginning of this section was created (Fig. 6). The severe weather

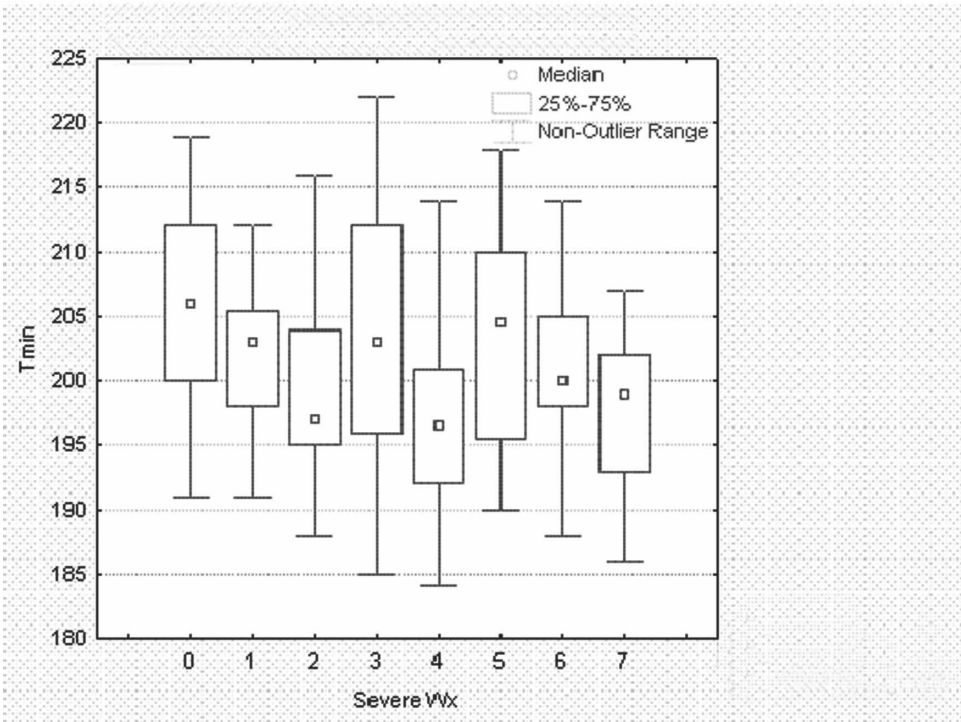

FIG. 6. TMIN box plot for all enhanced-V cases from the 2003 season for the eight severe weather categories. The severe weather categories are the same as those listed in Fig. 4. In addition, the median value of TMIN, the 25%–75% quartile ranges for TMIN, and the nonoutlier range for TMIN for each severe weather category are plotted.

categories of tornado, hail, and wind had the coldest median TMIN value [197 K (−76°C)] and coldest 25%–75% quartile TMIN values [192 K (−81°C) and 201 K (−72°C)]. However, the nonoutlier range overlapped all other severe weather categories, including the severe weather category of no tornado, hail, or wind. The severe weather category of no tornado, hail, or wind had the warmest median TMIN value [206.5 K (−66.5°C)] and the warmest 25%–75% quartile TMIN values [200 K (−73°C) and 212 K (−61°C)]. All of the other severe weather categories had median TMIN values and 25%–75% quartile TMIN values between the severe weather category of tornado, hail, and wind and the severe weather category of no tornado, hail, or wind. However, the 25% quartile TMIN value for the severe weather category of no tornado, hail, or wind was colder than the median TMIN value for many of the severe weather categories. Hence, TMIN alone is not adequate for distinguishing between enhanced-V cases that had severe weather associated with them and enhanced-V cases that did not have severe weather. The 2004 season box plot of TMIN values showed similar results.

A box plot of TDIFF values associated with enhanced-V cases from the 2003 season for the severe weather categories was also created (Fig. 7). The severe weather category of tornado, hail, and wind had the largest median TDIFF value (21 K) and largest 25%–75% quartile TDIFF values (16.5 and 25 K). However, the nonoutlier range overlapped all other severe weather categories, including the severe weather category of no tornado, hail, or wind. The severe weather category of no tornado, hail, or wind and the severe weather category of wind only had the smallest median TDIFF values (around 12 K for both) and the smallest 25%–75% quartile TDIFF values (10 and 15 K). All of the other severe weather categories had median TDIFF values and 25%–75% quartile TDIFF values between the severe weather category of tornado, hail, and wind and the severe weather categories of wind and no tornado, hail, or wind. The 75% quartile TDIFF value for the severe weather category of no tornado, hail, or wind was smaller than or equal to the median TDIFF values for all of the severe weather categories except wind only. Overall, the TDIFF box plot shows that there is a fairly good distinction between the TDIFF values associated with enhanced-V cases that had severe weather (other than just wind only) and enhanced-V cases that did not have severe weather. The TDIFF threshold for enhanced-V cases associated with severe weather ver-

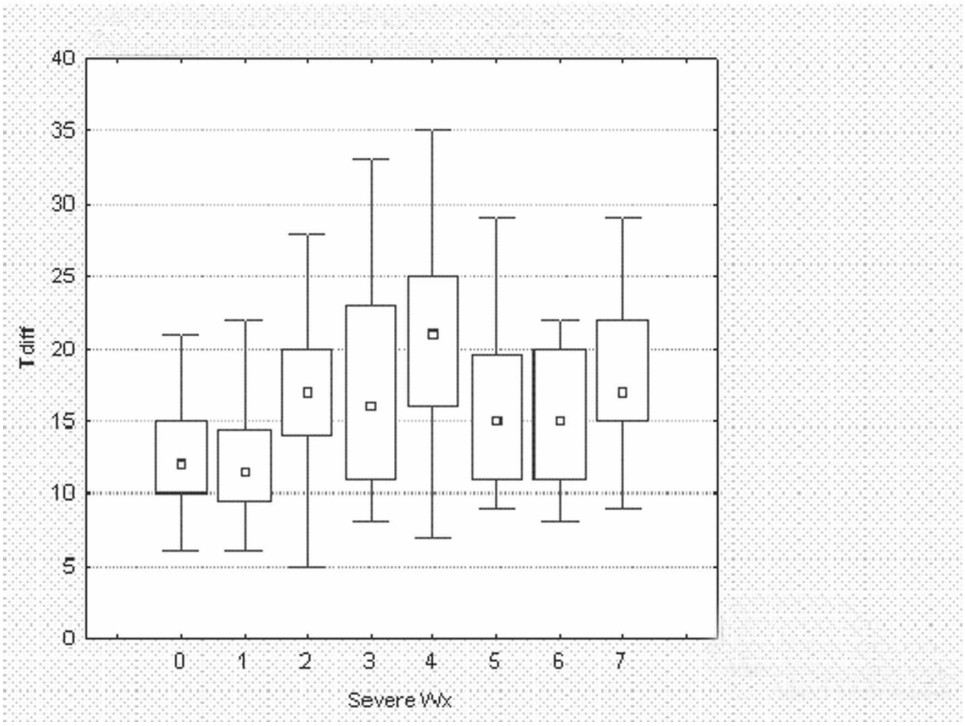

FIG. 7. Same as in Fig. 6 but for the TDIFF box plot.

sus enhanced-V cases not associated with severe weather seems to occur around 15 K. The 2004 season box plot of TDIFF values showed similar results.

c. *Upper-level wind speed and severe weather*

The upper-level wind speed (UL WIND SPD) from the GOES water vapor–derived winds (WVDW) was examined using a 1D scatterplot for all enhanced-V cases for the 2003 and 2004 seasons with severe weather categories plotted (Figs. 8 and 9). The UL WIND SPD at the near-tropopause level was examined instead of vertical wind shear because the enhanced-V feature occurs at the cloud top instead of throughout a deep layer of the storm. A UL WIND SPD of greater than 50 kt (26 m s^{-1}) was chosen as the threshold for the UL WIND SPD scatterplot. Some 93% and 99% of the enhanced-V cases that met the UL WIND SPD threshold had the "any of three severe types" category associated with them for the 2003 and 2004 seasons, respectively (Table 12). Enhanced-V cases that met the UL WIND SPD threshold had the largest association with severe hail for both seasons, while also having the lowest association with severe wind in the 2003 season and tornadoes in the 2004 season. The percent errors between the 2003 and 2004 seasons for the UL WIND SPD scatterplot were largest for severe hail and smallest for severe wind (Table 12). Overall, the percent error between the two seasons for the UL WIND SPD scatterplot for the any of three severe types category was 6%.

A forecaster could use the UL WIND SPD observed from the GOES WVDW as another key parameter for severe weather warning decision making because of the high probabilities of severe weather associated with enhanced-V cases that had UL WIND SPDs greater than 50 kt (26 m s^{-1}). An enhanced-V automated detection algorithm could also search for the nearest UL WIND SPD or an averaged number of surrounding UL WIND SPDs closest to the enhanced V from the GOES WVDW. The results from the UL WIND SPD scatterplots show that the UL WIND SPD may be even more important than the enhanced-V temperature parameters (TMIN, TMAX, and TDIFF) since the UL WIND SPD threshold applied to the enhanced-V cases had a higher probability of severe weather compared to the temperature parameter thresholds. However, the temperature parameters are still important in defining and detecting the enhanced V in the satellite imagery.

d. *Geographic and diurnal distributions of enhanced Vs*

Since there is a substantial association between severe weather and the enhanced-V feature shown in the last two sections and in many past papers (McCann

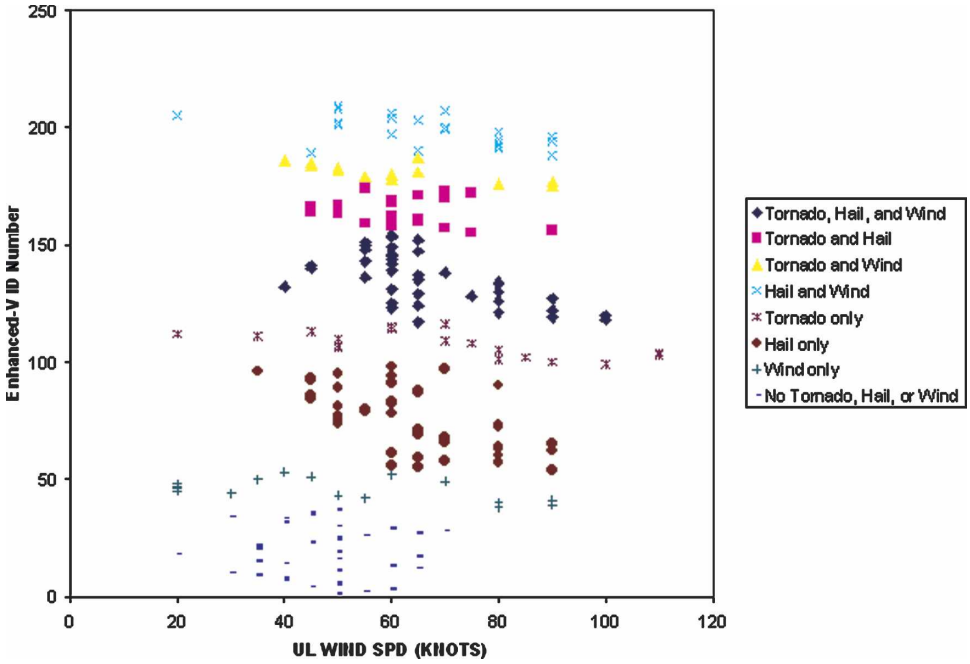

FIG. 8. A 1D scatterplot of UL WIND SPD (kt) for all enhanced-V cases in the 2003 season. Each enhanced-V case was assigned to one of eight severe weather categories: tornado, hail, and wind; tornado and hail only; tornado and wind only; hail and wind only; tornado only; hail only; wind only; and no tornado, hail, or wind.

1983; Negri 1982; Heymsfield et al. 1983a,b; Adler et al. 1985; Heymsfield and Blackmer 1988), it is hypothesized that the geographic distribution of enhanced-V features and severe weather should look similar. The majority of the enhanced-V cases (Fig. 10) occurred over the Great Plains and midwestern parts of the United States. With only a few reports of enhanced-V cases over the northeastern and western parts of the

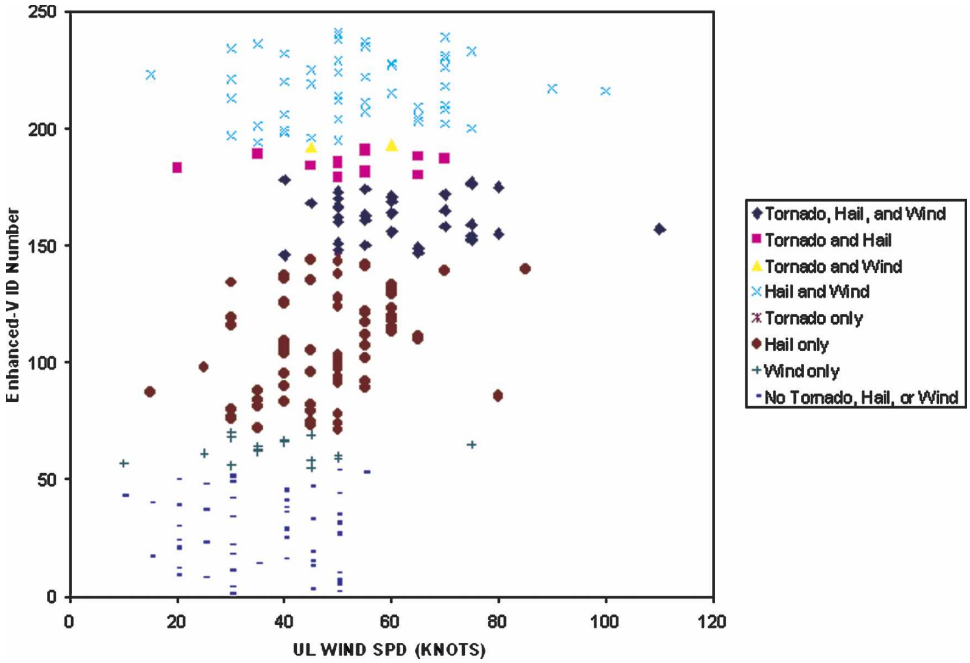

FIG. 9. Same as in Fig. 8 but for the 2004 season.

TABLE 12. Results from a 1D scatterplot of UL WIND SPD for the number of enhanced-V cases that met the UL WIND SPD threshold and that were associated with severe weather to the total number of enhanced-V cases that met the UL WIND SPD threshold. The severe weather categories included tornado, hail, wind, and any of three severe types for the 2003 and 2004 seasons. Also, the percent error between the 2003 and 2004 seasons is given for each severe weather category.

Severe weather category	2003 season	2004 season	Error (%)
Tornado	70/134 (52%)	30/82 (37%)	15
Hail	98/134 (73%)	79/82 (96%)	23
Wind	66/134 (49%)	47/82 (57%)	8
Any of three severe types	125/134 (93%)	81/82 (99%)	6

United States, there seems to be a high geographical distribution of enhanced-V cases to the Great Plains and midwestern climatic regions. However, since the two seasons include only LEO imagery, there may have been enhanced-V features that were not detected, because they occurred before or after the satellite overpass. In addition, the peak frequency for thunderstorms over the northeastern United States is during the month of July (Changnon 2001), so it is possible that there may have been a few more enhanced-V cases detected over the northeast United States if the datasets had included the entire month of July. Our datasets included data from early May to early July. However, the geographic distribution observed in our data is consistent with the distribution in previous studies of enhanced-V features. In past studies, almost every enhanced-V case study occurred over the Great Plains and midwestern parts of the United States (e.g., Adler et al. 1985; Heymsfield and Blackmer 1988; Heymsfield and Fulton 1994; Heymsfield et al. 1983a,b; McCann 1983; Negri 1982). In addition, compared to the rest of the United States, the Great Plains and Midwest are climatologically favored for deep convection and severe weather (Changnon 2001). The geographic distribution of enhanced-V features from this study and the severe weather climatology over the United States look similar. Therefore, the geographic distribution of enhanced-V features from this study supports the strong relationship between the enhanced-V features at cloud top and a reasonably high probability of observing severe weather.

In addition, it is hypothesized that the daytime versus nighttime satellite distribution of the enhanced-V fea-

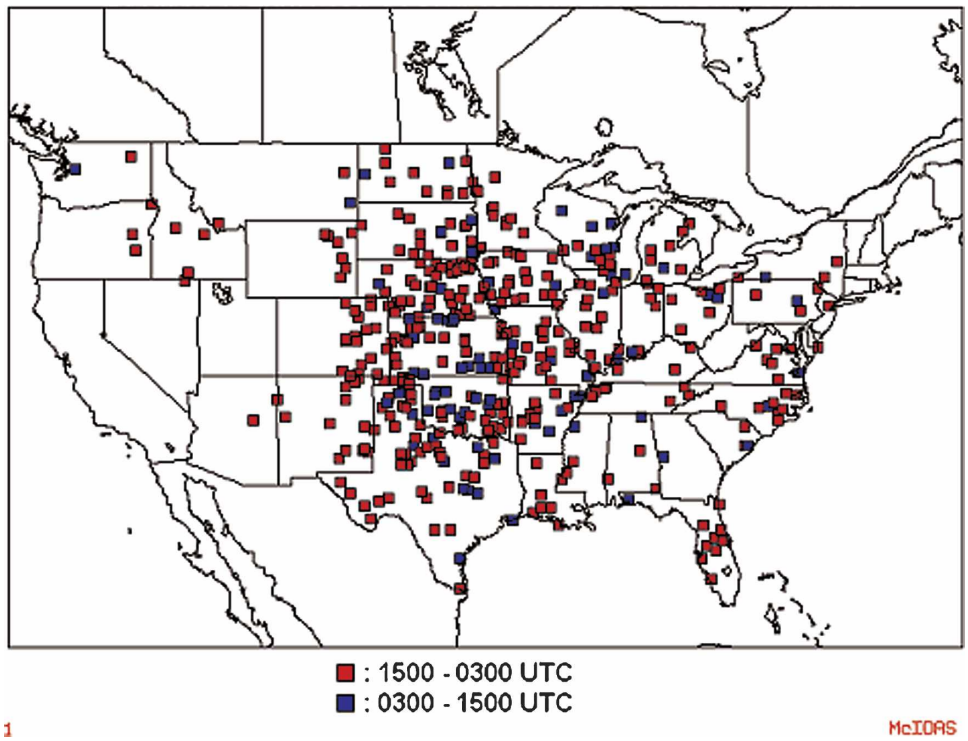

FIG. 10. Map showing the locations of the enhanced-V cases over the United States from the 2003 and 2004 seasons. The enhanced-V cases that are labeled in red occurred between 1500 and 0300 UTC (daytime and evening hours), while the enhanced-V cases that are labeled in blue occurred between 0300 and 1500 UTC (evening and daytime hours).

ture is similar to the daytime versus nighttime severe weather distribution. Enhanced-V cases that occurred between 1500 and 0300 UTC are considered daytime/evening convection, while enhanced-V cases that occurred between 0300 and 1500 UTC are considered nighttime/morning convection. There was a noticeable difference in the daytime versus nighttime satellite distribution of the enhanced-V features. Approximately 81% of the enhanced-V cases (366 out of 450 cases) for the two seasons occurred between 1500 and 0300 UTC. In addition, severe weather (i.e., especially tornadoes) usually occurs during the afternoon and evening hours (Ackerman and Knox 2003). The daytime versus nighttime distribution of enhanced-V features looks similar to the daytime versus nighttime distribution of severe weather. Therefore, the daytime versus nighttime satellite distribution of enhanced-V features from this study also supports the strong relationship between the enhanced-V features at cloud top and a reasonably high probability of observing severe weather.

6. Conclusions

This study investigated the enhanced-V feature at cloud top and its relationship to observing severe weather. The enhanced-V feature was observed with finer ground-sampled distance (i.e., 1 km) satellite imagery as compared to past enhanced-V studies and was investigated as a warning tool for severe weather. The results of verification statistics from this study were compared with McCann's (1983) enhanced-V study. These results showed that the probability of detection (POD) and critical success index (CSI) of enhanced-V features for forecasting severe weather were slightly better (increased a little), while the false alarm ratio (FAR) was slightly worse (increased a little) compared to McCann's study. However, if the constraint on the time of the severe reports with respect to the observation of the enhanced-V feature is loosened to within 3 h before or after the enhanced-V image time, then the FAR values for severe weather in general decreased to values slightly better than McCann's FAR. Overall, the increase in the POD for severe weather in general and especially tornadoes may have been a result of the finer ground-sampled distance (i.e., 1 km) used in this study compared to McCann's 8-km ground-sampled distance. However, the POD for significant tornadoes (50%) within this study (2003 season) was the same as that found by McCann.

The enhanced-V cases that met the TMIN and TMAX thresholds in the 2D scatterplot had high percentages (96% for 2003 season and 88% for 2004 season) of being associated with severe weather. Therefore, a forecaster could use TMIN and TMAX in a quantitative sense to distinguish the strength of a storm and in severe weather warning decision making since these parameters are linked to the strength of physical processes in deep convection. In addition, an enhanced-V automated detection algorithm could be developed to focus on the TMIN, TMAX, and TDIFF values and provide warnings to a storm if these values exceeded thresholds of 205 K (−68°C) for TMIN and 212 K (−61°C) for TMAX (implying larger TDIFF values). Also, the TDIFF box plot from the 2003 season showed that there is a fairly good distinction between the TDIFF values associated with enhanced-V cases that had severe weather (other than just wind only) and enhanced-V cases that did not have severe weather. The TDIFF threshold for enhanced-V cases associated with severe weather versus enhanced-V cases not associated with severe weather seems to occur around 15 K.

A forecaster could also use the upper-level wind speed (UL WIND SPD) observed from the Geostationary Operational Environmental Satellite (GOES) water vapor–derived winds (WVDWs) as another key parameter for severe weather warning decision making because of the high probabilities of severe weather (93% for 2003 season and 99% for 2004 season) associated with enhanced-V cases that had UL WIND SPDs greater than 50 kt (26 m s^{-1}). An enhanced-V automated detection algorithm could also search for the nearest UL WIND SPD or an averaged number of surrounding UL WIND SPDs closest to the enhanced V from the GOES WVDWs. The results from the UL WIND SPD scatterplots show that the UL WIND SPD may be even more important than the enhanced-V temperature parameters (TMIN, TMAX, and TDIFF) since the UL WIND SPD threshold applied to the enhanced-V cases had a higher probability of severe weather as compared to the temperature parameter thresholds. However, the temperature parameters are still important in defining and detecting the enhanced V in the satellite imagery.

This study focused on enhanced-V features observed with finer (1 km) ground-sampled distance but with very coarse temporal sampling. Therefore, the evolution of the enhanced-V parameters at 1-km ground-sampled distance could not be examined because of the poor temporal sampling. However, future satellites such as the Advanced Baseline Imager on board GOES-R will be able to monitor the temporal evolution of the enhanced-V parameters with 5-min interval data but with a slightly coarser ground-sampled distance (2 km) compared to LEO satellite imagery

(Schmit et al. 2005). The ideal satellite to improve the detection of severe weather with enhanced-V features further should have the highest available temporal sampling (such as 1-min interval data) but with a ground-sampled distance (1 km) similar to that was used in this study. Future studies should also examine values of the enhanced-V parameters with current GOES data and compare those results to the values of the parameters observed in LEO satellite data. Also, the time evolution of the enhanced-V parameters with current GOES data should be investigated to see if trends in the parameters could be used in severe weather warning decision making.

Acknowledgments. The archived LEO NOAA-AVHRR overpasses were obtained from the Satellite Active Archive (SAA) and the archived LEO EOS MODIS *Aqua* and *Terra* overpasses were obtained from the Goddard Space Flight Center (GSFC) Distributed Active Archive Center (DAAC). GOES WVDWs were provided by the Cooperative Institute for Meteorological Satellite Studies (CIMSS) at the University of Wisconsin—Madison. These upper-level wind speeds and directions were estimated from the automated satellite winds algorithm developed at CIMSS. Archived raobs were obtained from the Department of Atmospheric Science at the University of Wyoming.

REFERENCES

Ackerman, S. A., and J. A. Knox, 2003: Thunderstorms and tornadoes. *Meteorology: Understanding the Atmosphere,* K. Dodson et al., Eds., Brooks/Cole, 306–337.

Adler, R. F., and R. A. Mack, 1986: Thunderstorm cloud top dynamics as inferred from satellite observations and a cloud top parcel model. *J. Atmos. Sci.,* **43,** 1945–1960.

——, M. J. Markus, D. D. Fenn, G. Szejwach, and W. E. Shenk, 1983: Thunderstorm top structure observed by aircraft overflights with an infrared radiometer. *J. Appl. Meteor.,* **22,** 579–593.

——, ——, and ——, 1985: Detection of severe Midwest thunderstorms using geosynchronous satellite data. *Mon. Wea. Rev.,* **113,** 769–781.

Brunner, J. C., 2004: A quantitative analysis of the enhanced-V feature in relation to severe weather. M.S. thesis, Dept. of Atmospheric and Oceanic Sciences, University of Wisconsin—Madison, 96 pp.

Changnon, S. A., 2001: *Thunderstorms across the Nation: An Atlas of Storms, Hail, and Their Damages in the 20th Century.* Changnon Climatologist, 93 pp.

Clark, J. D., Ed., 1983: The GOES user's guide. NOAA Rep. NOAA83093001, Washington, DC, 167 pp.

Fujita, T. T., 1974: Overshooting thunderheads observed from ATS and Learjet. Satellite and Mesometeorology Research Project Rep. 117, Texas Tech University, Lubbock, TX, 29 pp.

——, 1978: Manual of downburst identification for Project NIMROD. Satellite and Mesometeorology Research Project Rep. 156, University of Chicago, Chicago, IL, 104 pp.

——, 1982: Principle of stereoscopic height computations and their applications to stratospheric cirrus over severe thunderstorms. *J. Meteor. Soc. Japan,* **60,** 355–368.

Gunshor, M. M., T. J. Schmit, and W. P. Menzel, 2004: Intercalibration of the infrared window and water vapor channels on operational geostationary environmental satellites using a single polar-orbiting satellite. *J. Atmos. Oceanic Technol.,* **21,** 61–68.

Heymsfield, G. M., and R. H. Blackmer Jr., 1988: Satellite-observed characteristics of Midwest severe thunderstorm anvils. *Mon. Wea. Rev.,* **116,** 2200–2224.

——, and R. Fulton, 1994: Passive microwave structure of severe tornadic storms on 16 November 1987. *Mon. Wea. Rev.,* **122,** 2587–2595.

——, R. H. Blackmer Jr., and S. Schotz, 1983a: Upper-level structure of Oklahoma tornadic storms on 2 May 1979. I: Radar and satellite observations. *J. Atmos. Sci.,* **40,** 1740–1755.

——, G. Szejwach, S. Schotz, and R. H. Blackmer Jr., 1983b: Upper-level structure of Oklahoma tornadic storms on 2 May 1979. II: Proposed explanation of "V" pattern and internal warm region in infrared observations. *J. Atmos. Sci.,* **40,** 1756–1767.

——, R. Fulton, and J. D. Spinhirne, 1991: Aircraft overflight measurements of Midwest severe storms: Implications on geosynchronous satellite interpretations. *Mon. Wea. Rev.,* **119,** 436–456.

Lazzara, M. A., and Coauthors, 1999: The Man computer Interactive Data Access System: 25 years of interactive processing. *Bull. Amer. Meteor. Soc.,* **80,** 271–284.

McCann, D. W., 1983: The enhanced-V: A satellite observable severe storm signature. *Mon. Wea. Rev.,* **111,** 887–894.

Menzel, W. P., and J. F. Purdom, 1994: Introducing GOES-I: The first of a new generation of Geostationary Operational Environmental Satellites. *Bull. Amer. Meteor. Soc.,* **75,** 757–781.

Miller, L. J., J. D. Tuttle, and G. B. Foote, 1990: Precipitation production in a large Montana hailstorm: Airflow and particle growth trajectories. *J. Atmos. Sci.,* **47,** 1619–1646.

Negri, A. J., 1982: Cloud-top structure of tornadic storms on 10 April 1979 from rapid scan and stereo satellite observations. *Bull. Amer. Meteor. Soc.,* **63,** 1151–1159.

Rabin, R. M., S. F. Corfidi, J. C. Brunner, and C. E. Hane, 2004: Detecting winds aloft from water vapour satellite imagery in the vicinity of storms. *Weather,* **59,** 251–257.

Schaefer, J. T., 1990: The critical success index as an indicator of warning skill. *Wea. Forecasting,* **5,** 570–575.

Schlesinger, R. E., 1984: Mature thunderstorm cloud-top structure and dynamics: A three-dimensional numerical simulation study. *J. Atmos. Sci.,* **41,** 1551–1570.

Schmit, T. J., M. M. Gunshor, W. P. Menzel, J. J. Gurka, J. Li, and A. S. Bachmeier, 2005: Introducing the next-generation Advanced Baseline Imager on GOES-R. *Bull. Amer. Meteor. Soc.,* **86,** 1079–1096.

Setvak, M., R. M. Rabin, and P. K. Wang, 2007: Contribution of the MODIS instrument to observations of deep convective storms and stratospheric moisture detection in GOES and MSG imagery. *Atmos. Res.,* **83,** 505–518.

Stobie, J. G., 1975: Gravity shear waves atop the cirrus layer of

intense convective storms. NASA Contractor Rep. NASA-CR-147140, Colorado State University, Fort Collins, CO, 128 pp.

Tobin, D. C., H. E. Revercomb, C. C. Moeller, and T. S. Pagano, 2006: Use of Atmospheric Infrared Sounder high–spectral resolution spectra to assess the calibration of Moderate resolution Imaging Spectroradiometer on EOS Aqua. *J. Geophys. Res.,* **111,** D09S05, doi:10.1029/2005JD006095.

Wang, P. K., 2007: The thermodynamic structure atop a penetrating convective thunderstorm. *Atmos. Res.,* **83,** 254–262.

——, H.-M. Lin, S. Natali, S. Bachmeier, and R. Rabin, 2002: Cloud model interpretation of the mechanisms responsible for the satellite-observed enhanced V and other features atop some Midwest severe thunderstorms. Preprints, *11th Conf. on Cloud Physics,* Ogden, UT, Amer. Meteor. Soc., CD-ROM, 1.2.